Influence of laser structural patterning on the tribological performance of C-alloyed W-S coatings

Mohammadreza Shamshiri, Ana Manaia, Todor Vuchkov, Alexandre Carvalho, Guilherme Gaspar, António Fernandes, Samaneh Heydarian Dolatabadi, Florinda Costa, Albano Cavaleiro

PII: S0257-8972(20)30491-6

DOI: https://doi.org/10.1016/j.surfcoat.2020.125822

Reference: SCT 125822

To appear in: *Surface & Coatings Technology*

Received date: 8 February 2020

Revised date: 19 April 2020

Accepted date: 20 April 2020

Please cite this article as: M. Shamshiri, A. Manaia, T. Vuchkov, et al., Influence of laser structural patterning on the tribological performance of C-alloyed W-S coatings, *Surface & Coatings Technology* (2020), https://doi.org/10.1016/j.surfcoat.2020.125822

Influence of laser structural patterning on the tribological performance of C-alloyed W-S coatings

Mohammadreza Shamshiri [a*], Ana Manaia [b], Todor Vuchkov [ab], Alexandre Carvalho [c], Guilherme Gaspar [c], António Fernandes [c], Samaneh Heydarian Dolatabadi [d], Florinda Costa [c], Albano Cavaleiro [ab]

[a] SEG-CEMMPRE, Department of Mechanical Engineering, University of Coimbra, Rua Luís Reis Santos, 3030-788 Coimbra, Portugal

[b] IPN - LED & MAT - Instituto Pedro Nunes, Laboratory for Wear, Testing and Materials, Rua Pedro Nunes, Coimbra, Portugal

[c] Physics Department & i3N, University of Aveiro, Campus Universitário de Santiago, 3810-193 Aveiro, Portugal

[d] Department of Applied Sciences, University of Quebec in Chicoutimi (UQAC), 555, boul. de l'Université, Chicoutimi, Quebec, G7H 2B1, Canada

* Corresponding author: E-mail address: mshamshiri@student.dem.uc.pt

Abstract

In this paper, we are proposing for the first time the partial laser treatment of a self-lubricating coating in order to optimize its frictional performance from the very first moments of the sliding contact. W-S films alloyed with carbon were deposited by closed field unbalanced magnetron sputtering. The coatings were treated using two types of lasers, with peak emissions in the UV and IR, under different laser power conditions and patterning. The structure, mechanical and tribological properties of the treated coatings were analysed using X-ray diffraction (XRD), Raman spectroscopy, nanoindentation and reciprocating ball-on-disk tribometry. Although XRD diffractograms illustrated an overall amorphous structure in all as-deposited and treated samples, their Raman spectra confirmed the presence of WS_2 crystalline phase in some of the treated areas. Furthermore, in the samples where WS_2 Raman peaks were detected, the friction coefficient was in the initial part of the test lower than that of untreated coating. Previous crystallization of the W-S phase before tribological testing has a key role for shortening the self-adaption process improving the overall friction performance of the coatings.

Keywords: Transition Metal Dichalcogenides; Laser treatment; Magnetron sputtering; Self-lubrication; Tribolayer

1. Introduction

Energy dissipation and material loss, both issues related to friction and wear, have attracted many attentions in the last decades [1,2,3]. The use of liquid lubricants has been always considered as an effective solution to control the coefficients of friction and wear. However, their drawbacks such as contaminations, low thermal resistance and, recently, environmental issues have raised the demand for solid lubricants. In fact, by generating a tribofilm, these lubricants can provide steady low friction values keeping the components undamaged under high loads and high temperatures [4,5].

Transition metal dichalcogenides (TMDs) are known as layered materials where strong bonding exists within the layer, while the interaction between layers is related to the weak Van der Waals forces [4, 6, 7]. These layered materials are commonly used as either oil additives or coatings to reduce the friction [5]. When a shear force is applied to TMDs, the basal planes slide over each other due to the easy inter-crystalline slip and, under repeated sliding condition, the layers can move considerable distances. The lubricating mechanism of TMDs is described by this freely movement of adjacent layers [4,8,9].

There are several criteria for a coating to be considered as a good solid lubricant, including the sufficient adhesion between the lubricant and the substrate, the good internal cohesion of the coating and a low adhesion between the particles and layers in the shearing direction [10]. Due to the columnar and porous structure, TMDs, such as tungsten disulphide (WS_2), are prone to failure and, thus, an enhancement of their mechanical properties is required. Alloying the TMDs with elements, such as N and C, is one of the widespread procedures to prevent the formation of the large-sized grains in the structure and to stop the columnar growth; usually this type of alloying results in a decrease of the coatings crystallinity or, even, in an amorphous structure [11,12,13]. However, this structure could usually cause difficulties in promoting the self-adaption process, thus requiring long running times at low applied loads or high loads to trigger the lubricating phenomenon. This is crucial in applications in contact with rubber, where the contact loads are very low, requiring an alternate way to induce this process. The formation of crystalline WS_2 would be a simple and effective way.

Among all treatment procedures, the laser treatment is a well-known surface treatment technique which can provide control over various parameters in a very accurate and efficient way [14,15,16,17]. This technique has been utilized to enhance the crystallinity and orientation of TMDs such as molybdenum disulphide [18,19]. The main advantage of the laser treatment would be the possibility to treat small volumes (e.g. ~20%) of the coating without significantly altering the overall mechanical properties of the films. The treated areas can act as reservoirs rich in more crystalline lubricious TMD phase. During sliding, the lubricious TMD phase, originated from the treated zones, can be smeared in the direction of sliding while the untreated areas can provide the load bearing capacity. This process leads to an advantageous sliding scenario where the low shear strength of the sliding interface is governed by the crystalline TMD phase while the load bearing capacity is provided by the harder untreated areas.

For the purpose of accelerating the formation of lubricious tribofilms and hence the running-in behaviour, different laser treatments were performed on quasi-amorphous W-S-C coatings. The crystallinity, mechanical and tribological properties were studied as a function of the treatment process.

2. Experimental

The coatings were deposited by close field unbalanced magnetron sputtering from C, WS_2 and Cr targets using a UDP 650/4 Teer Coatings deposition equipment (Teer Coatings Limited). Before the process, in order to obtain smoother surfaces and better coating adhesion, the M2 steel substrates were polished to a roughness of Ra < 20 nm using SiC papers and diamond suspension with a particle size of 3μm, ultrasonically cleaned with ethanol and then placed in a rotating substrate holder at a target-to-substrate distance of 25 cm. The chamber was evacuated down to 5×10^{-4} Pa. Before the deposition, the substrates were sputter cleaned in an argon atmosphere for 40 min using pulsed-DC current (Advanced Energy Pinnacle Plus) at a bias voltage of 600V, frequency of 250 kHz and reverse time of 1.6μs. The targets were sputter cleaned for 20 min each, with the DC (Advanced Energy Pinnacle) power applied resulting in power density of 2.1 $W.cm^{-2}$.

The process starts with the deposition of a Cr interlayer (~200-300 nm) to promote the adhesion between the substrate and the coating. Afterwards, a gradient layer (~100nm) was deposited by simultaneously decreasing the power on the Cr target and increasing the powers on the WS_2 and graphite targets. The amount of carbon used as addition was selected based

on previous studies [5]. The addition of ~50 at. % of carbon usually results in coatings with moderate hardness and moderate contents of a lubricious TMD phase. For achieving this level of carbon content, 1 WS_2 and 2 graphite targets were used. The power density applied to the WS_2 was 2.1 $W.cm^{-2}$, while the power density applied to both graphite targets was set to 3.2 $W.cm^{-2}$. The deposition was performed in Ar atmosphere at a pressure of ~0.4 Pa. The whole deposition process lasted for 2 hours.

A field emission scanning electron microscope (FESEM, Zeiss Merlin) was used to observe the cross-sectional morphology of the coating as well as to analyse its chemical composition by wavelength dispersion spectroscopy (WDS, Oxford Instruments). Energy-dispersive spectroscopy (EDS) was performed using a detector (Oxford Instruments) attached to the FESEM. The EDS analysis was performed using an accelerating voltage of 15 kV.

Two different types of laser, namely ultra-violet (UV) and infra-red (IR), neodymium-doped yttrium aluminium garnet (Nd:YAG), were used to treat the samples. The pulsed Nd:YAG (1064 nm wavelength), model Starmark SMP from Rofin, is equipped with a galvanometric head and a F-theta lens (100 mm focal distance) to allow processing of centimetre-size samples. The distance between scan lines was set to 100 µm, being the minimum allowed by the apparatus, while fast scan speeds and both low laser powers and pulsing frequencies were explored in the context of this work. To reduce power density delivered to the thin film coatings, defocusing conditions were attempted. Before laser scanning, some of the samples (YAG2 and YAG3) were covered with a suitably designed mask (regular grid with 15 µm diameter holes) to constrain the laser-treated areas as a requirement for the tribological analyses. It should be noted that the laser used in this task exhibited low stability for low powers, the ones required for the laser treatment of these samples. Therefore, higher power than required was used; however, to keep the intensity below the graphitization threshold, the beam was defocused at the sample. Furthermore, as the objective in this work was to produce a laser-treated pattern, masking can be a strategy to achieve it. In addition, by defocusing the laser. the spot size at the sample is drastically enlarged, ruining the laser scribing resolution. Thus, using the mask, the uniformity was also improved. The laser processing conditions with the Nd:YAG laser are summarised in Table 1.

A diode-pumped pulsed UV (355 nm) Inngu Laser, with maximum power of 3W fitted with a scan head with a F-theta lens (160 mm focal distance, 100×100 mm^2 max. scanned area), was used to assess the impact of wavelength on the coating phase transformation. By varying

laser parameters, the coating surface could be almost completely treated, or a dot pattern could be achieved. The UV1 treatment consisted of a rectangular grid type dot pattern, with the distance between the dots (centre to centre) being ~ 20 x 40 μm. The experimental conditions and characteristics of all treated samples are illustrated in Table 1.

Table 1. Experimental conditions and characteristics of the laser-treated samples.

Sample	Pattern	Distance to focal plane [mm]	Laser power [mW]	Scan speed [mm.s^{-1}]	Pulsing frequency [kHz]	Affected area [%]
YAG1	Without mask	30	4.5	2000	4	-
YAG2	With mask	30	4.5	2000	4	17
YAG3	With mask	25	4.5	2000	4	17
UV1	Dots	0	4	100	75	20
UV2	Compact dots	0	30	1000	75	>70

A ZEISS Axio Imager Z2m optical microscope was used for the initial investigation of the samples. All samples were characterized by micro- Raman analysis, performed in backscattering configuration on a Horiba HR800 instrument using a 600 lines mm^{-1} grating and the 441.6 nm laser line from a HeCd laser (Kimmon IK Series, Japan) with an OD 2 ND filter to prevent the laser from changing the sample structure.

The structure of the coatings was accessed in a Philips (PANalytical) diffractometer with Co-Kα radiation (λ = 0.17902 nm) in conventional (θ-2θ) mode. The scan step size was 0.025degrees with 2 seconds exposition per step.

A NanoTest Nanoindenter from Micro-Materials Ltd. was used to measure hardness of the samples using a Berkovich diamond pyramid indenter. 20 different tests with a 3 mN load were performed at room temperature (23^{o}C).

Reciprocating ball-on-disk tribological tests were performed in an Optimol SRV machine. The counterbody was a 10 mm 100Cr6 bearing steel ball. The applied load was 5 N (initial maximum contact pressure of ~813 MPa) and the tests had a 10 min duration. The frequency was set to 25 Hz with a stroke length of 2 mm, resulting in an average sliding speed of 0.1 m/s. To determine the wear rates of samples, 2D profiles of the wear track were obtained using a Bruker Alicona Infinite Focus 3D profilometer. The specific wear rate (W_r) was calculated according to Eq. 1.

$$W_r = \frac{V_w}{F \cdot s} \quad (1)$$

Where V_w is the wear volume (mm^3), F is the normal load (N) and s (m) is the sliding distance [20]. The tribological tests were performed twice per treatment.

3. Results and Discussion

3.1. Chemical Composition, Structure and Mechanical Properties

SEM analysis of the fractured cross section of the untreated W-S-C sputtered coating, depicted in Fig. 1, shows a rather compact, almost featureless coating with a total thickness of about 1.5µm. The elemental chemical composition of this coating was determined by WDS analysis and it is shown in Table 2. The carbon content of the film was approximately 47 at. %.

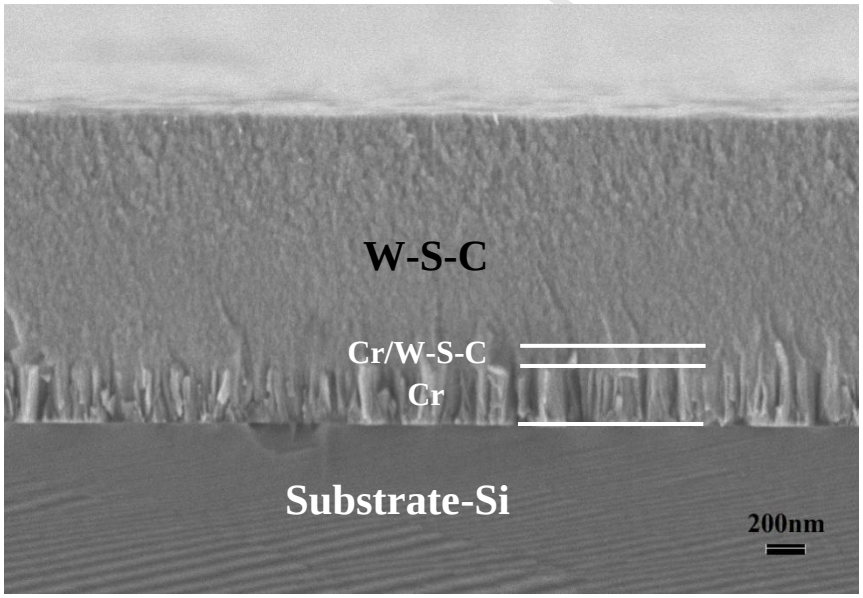

Fig. 1. Cross-sectional FESEM micrograph pf the untreated W-S-C sputtered coating.

Table 2. Chemical composition and thickness of W-S-C coatings.

Coating	Chemical composition [at. %]					Thickness [µm]
	W	Cr	S	O	C	
W-S-C	17.2	0.8	29.3	5.0	47.6	1.5

Fig. 2 shows the XRD diffractograms of the treated samples. Only a broad peak (2θ ~35 -50°) could be detected in all samples, suggesting that the coatings have an amorphous structure. This broad peak is often associated with the (100) reflection of WS_2, with the tail towards higher 2θ values representing turbostratic stacking of the (10L) planes, with L having values of 1,2,3,4 [21]. Nevertheless, even if these crystals are present, they are too small to be detected by XRD. This result is in agreement with previous results on the development of W-S-C coatings [22, 23]. UV2 sample shows badly defined features superimposed to the broad peak which can be associated with signs of crystallinity. According to Table 1, the total treated area in most of the samples is less than 20% of the original surfaces; therefore, any possible peak related to structural transformation, as will be shown later, would be overshadowed by the broad peak, due to low amount of crystalline material. In the case of UV2, with a treated area of more than 70% of its total surface, a narrower peak around 2θ~43° occurs. As it will be discussed later, this sample was over exposed to laser treatment with a strong graphitization taking place. However, this peak cannot be indexed to any form of carbon. Further studies will be necessary for this identification.

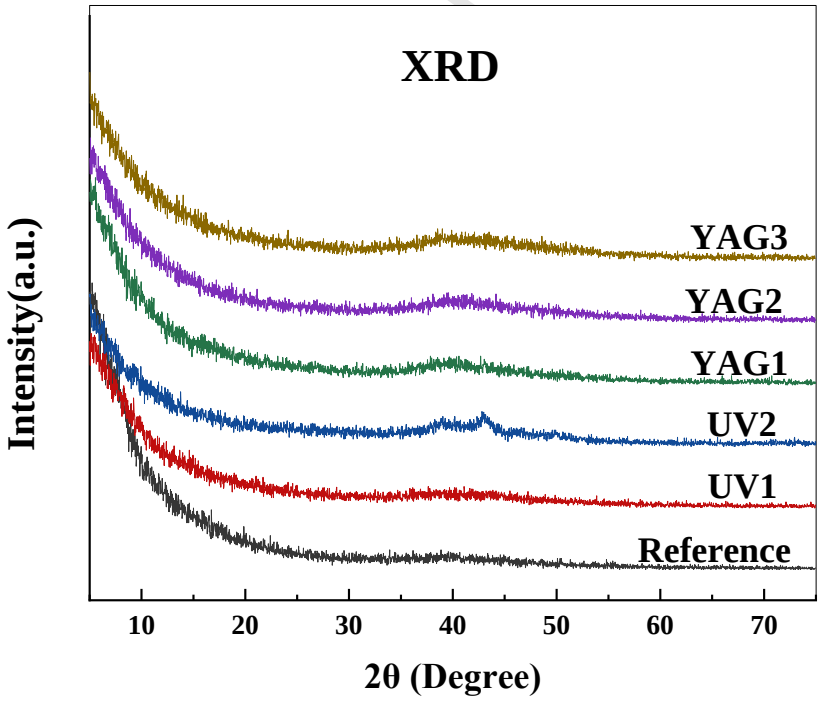

Fig. 2. The XRD patterns of all the laser-treated and untreated samples.

Fig. 3 shows optical micrographs of the two UV-treated samples. As expected, UV1 displays the dot-like pattern with each dot corresponding to a laser pulse. UV2 shows superimposed dots filling in almost the whole surface. In both micrographs different tonalities can be identified in the treated zones with a gradient from light to very dark grey, possibly associated with phase changes. Although the experimental conditions were kept constant, regrettably, local changes were observed on the laser-treated surface. The UV laser used in this work is characterized by a quite narrow field depth. Considering this, together with some topographic heterogeneities of the surface, different laser/matter interaction effects could be caused, as seen in Fig. 3(a). Since Raman spectroscopy is a well-known technique, adequate to locally identify phase transformations, spectra were taken from different points on UV1 (points 1,2 and 3) and UV2 (points 1 and 2) samples. These spectra are shown in Fig. 3 along with the reference spectrum taken from the as-deposited sample. In fact, the laser treatment induced a transformation in the carbon phase, corresponding to the splitting of the typical amorphous wide asymmetric single band into its two components, the D and the G bands. This becomes notorious as the spectrum of reference sample contains only one feature, that of the unsplitted amorphous carbon broad band. According to the literature, changing amorphous carbon into nanocrystalline graphite would cause the G peak to move from ~1510 cm^{-1} towards ~1600 cm^{-1} along with an increase in the $I(D)/I(G)$ ratio [24,25], as seen in the spectra took from spots where graphitisation occurred. This graphitisation phenomenon corresponds to a topological re-ordering of the amorphous sp^2 coordinated carbon structure. In this process, the carbon bonds become stronger therefore increasing the energy of the E_{2g} C-C stretching mode vibration in the sp^2 hybridisation.

The comparison between the reference and the UV1 spectra shows the narrowing of the D and G bands, their separation and a shift of G band to higher wavenumbers occurred, evidencing graphitisation. In the darker grey zones, a progressive over exposure of the material to the laser beam took place and consequently a higher crystallisation degree (point 3-UV1 and point 2-UV2).

The samples where graphitisation seems less pronounced exhibit two narrow peaks in the low wavenumber region (point 1-UV1 and point 1-UV2). These correspond to crystalline WS_2 vibration modes at ~356 cm^{-1} (E^1_{2g}) and ~421 cm^{-1} (A_{1g}) [26], showing that the laser incidence promoted the crystallization of WS_2. It is interesting to note that the WS_2 peaks intensity decreases with the increase of the D and G bands. As referred above, the latter bands are characteristic of a strong graphitisation of the carbon phases. Since the darkest grey is

predominant in the UV2 sample, the graphitic zones become dominant. The detection of crystalline WS_2 in the lighter zones of UV2 sample suggests that the laser local intensity was strong enough to produce WS_2 crystallization but still below the graphitisation threshold, while showing that the whole surface was treated. The 70% value shown in Table 1 refers to the dark grey area.

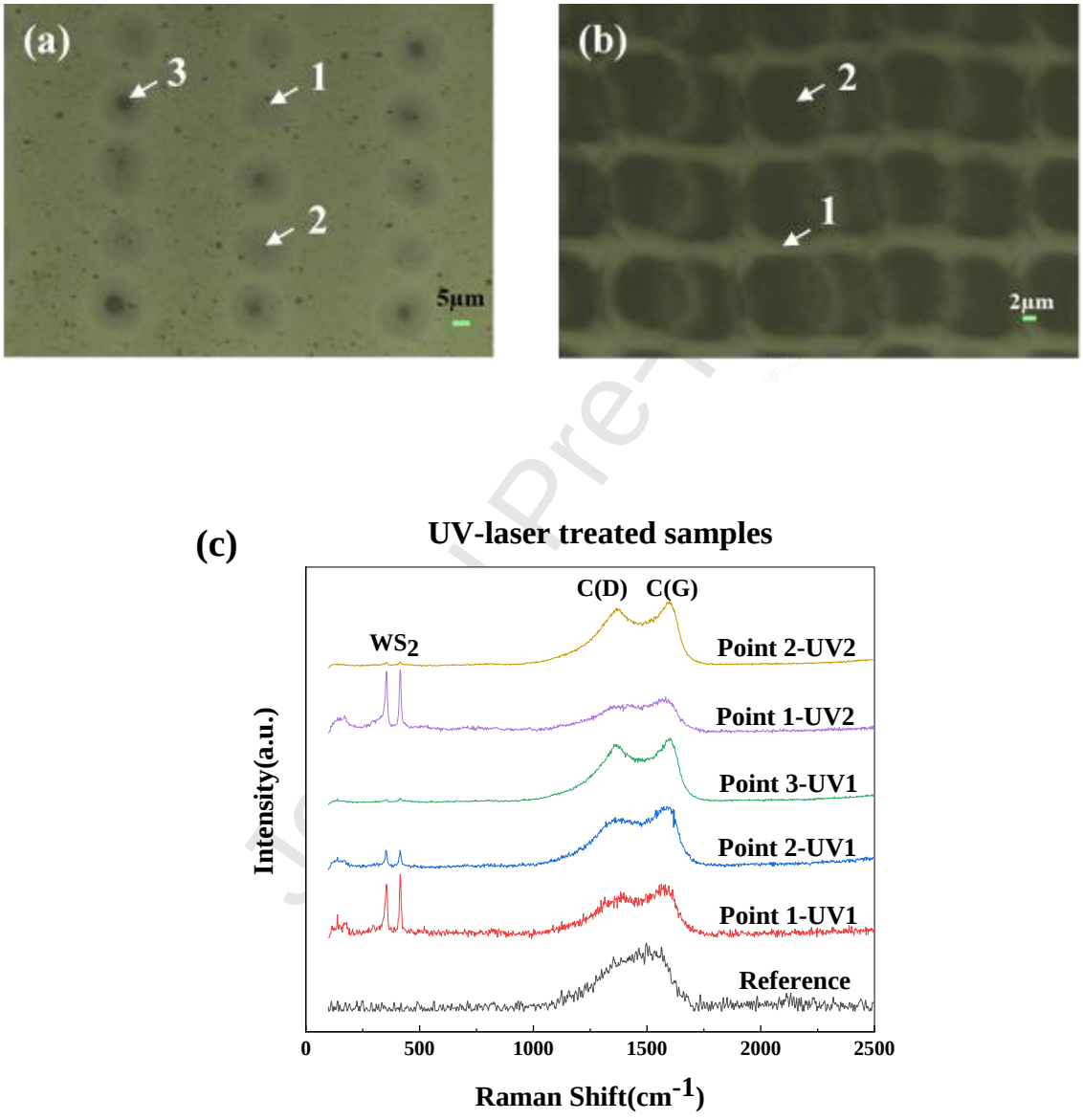

Fig. 3. The optical micrographs of (a) UV1 and (b) UV2 along with (c) their Raman spectra.

The main difference between YAG1 and YAG2 treatments is the featureless appearance of the surface treated with the YAG1 conditions. This treatment was performed without a mask

and all surface was homogeneously irradiated due to the defocusing conditions. The observation under an optical microscope revealed only weak grey tonalities. For YAG-treated samples, as would be expected since treating conditions were alike, the Raman spectra of four randomly selected points on YAG1 surface, as well as four points in the centre of treated dots in YAG2 sample, were similar (see Fig. 4). The crystallization of the originally amorphous W-S material also occurred in the treated zone. In fact, the two distinctive peaks of WS_2 at 356 and 421 cm^{-1} are patent, along with the carbon D and G bands. Again, the narrowing and separation of the D and G peaks and shifting of G peak towards higher wavenumbers indicate a slight graphitisation in the irradiated areas of this samples. Therefore, according to the Raman data, the degree of material treatment is comparable to that occurred in the lighter zones of UV-laser samples.

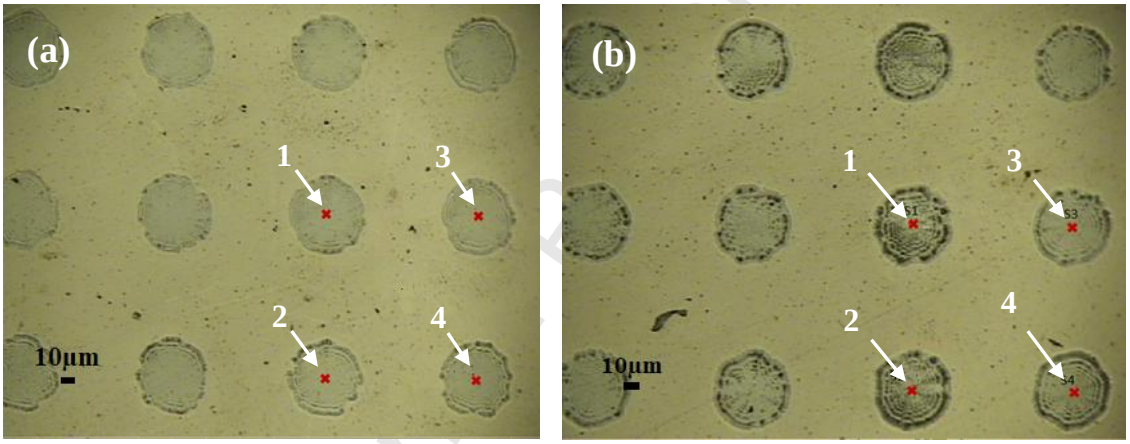

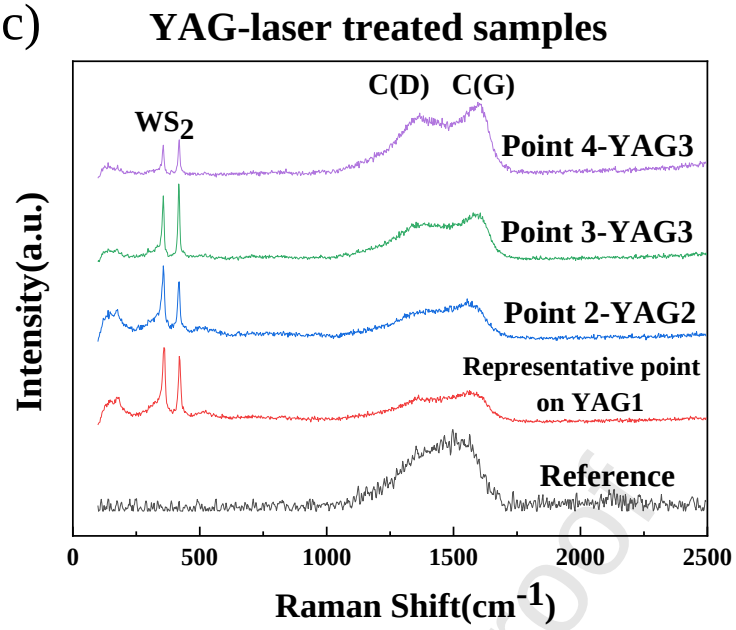

Fig. 4. The optical micrographs of YAG2 (a) and YAG3 (b) along with the Raman spectra of all YAG-laser treated samples(c).

As the YAG3 sample distance to the laser head was reduced in 5 mm, this sample was irradiated closer to the focus compared to YAG2, with the consequent intensity increase at the irradiated region. As observed in Fig. 4, radial patterns consisting of different grey tonalities are visible in each spot. Raman acquisitions performed in different zones in these spots corroborate the relation found for UV-treated samples. In fact, in lighter grey zones WS_2 crystallization occurred without noticeable changes in the carbon phase. Then, with the increase in the grey darkening, a progressive vanishing of the peaks corresponding to crystalline WS_2 phase, with a simultaneous increase in the C-phase graphitisation, took place. The radial aspect can be attributed to the diffraction effect caused by laser interaction with the mask, resulting in typical concentric annular patterns. This comes from the out-of-focus operation mode used in the masked samples, in which the irradiated region was much larger than the metallic mask apertures. The WS_2 crystallization and graphitization can be concurrent, i.e. small changes could always be observed by Raman in both characteristic peaks of W-S and C phases. However, depending on the laser intensity, sometimes the changes were almost imperceptible. For low laser intensity strong transformations could be observed for W-S phase whereas for C-based material almost no changes were detected (see for example Point 2 in Fig. 4c). High exposure would very likely cause oxidation of WS_2;

however, as Raman Spectroscopy did not show any peaks related to W-oxides, oxidation could not be confirmed for the current intensities used. The chemical analysis was performed in some areas and, in general, the treated zones contained more oxygen (based on EDS analysis) whereas little changes are registered for the S/W ratio. As an example, Fig. 5 illustrates EDS analysis performed in untreated and treated zones, in the wear track of the YAG3 sample.

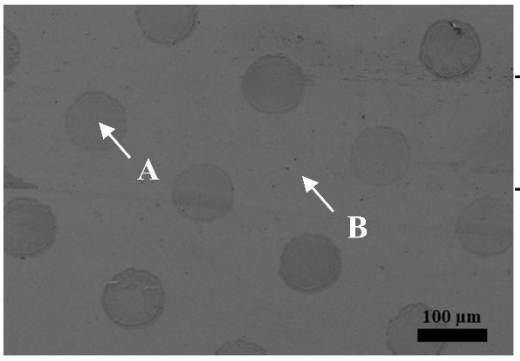

Zone	Chemical composition [at. %]				
	W	S	O	C	S/W
A	15.1	18.5	12.4	53.9	1.22
B	15.3	17.7	1.9	65.1	1.15

Fig 5. Chemical composition of the treated (A) and untreated (B) zones on YAG3.

The topography of the surfaces is presented in Fig. 6. Kononenko et al. [27] proposed 3 different intensity related processes during laser treatment of a-C coatings. At low intensities, there is a surface swelling in the irradiated zones due to the reduction of the density of the graphitised volumes. At increased intensities, multilevel spallation can occur. The process observed at the highest laser intensities is evaporation and subsequent formation of craters. In the present study, the only topographical feature observed in the irradiated zones is a small surface swelling. In the case of the UV1 treatment, the swollen areas have a height between 150 and 200 nm. The UV2 treatment resulted in features with similar height as the UV1 one, with the difference being larger irradiated areas (>70 %). The topography of the YAG1 sample did not have any specific features, since the whole area was homogeneously irradiated, resulting in a more featureless appearance. For the YAG2 and YAG3 samples, the topographical measurements were performed on a single treated area. YAG2 treatment resulted in smaller surface swelling compared to the YAG3 one. The highest features observed have a value of ~150 and ~250 nm for YAG2 and YAG3, respectively. As discussed previously, the YAG3 treatment was performed closer to the focal distance, causing laser irradiation with increased intensity and hence increased graphitisation.

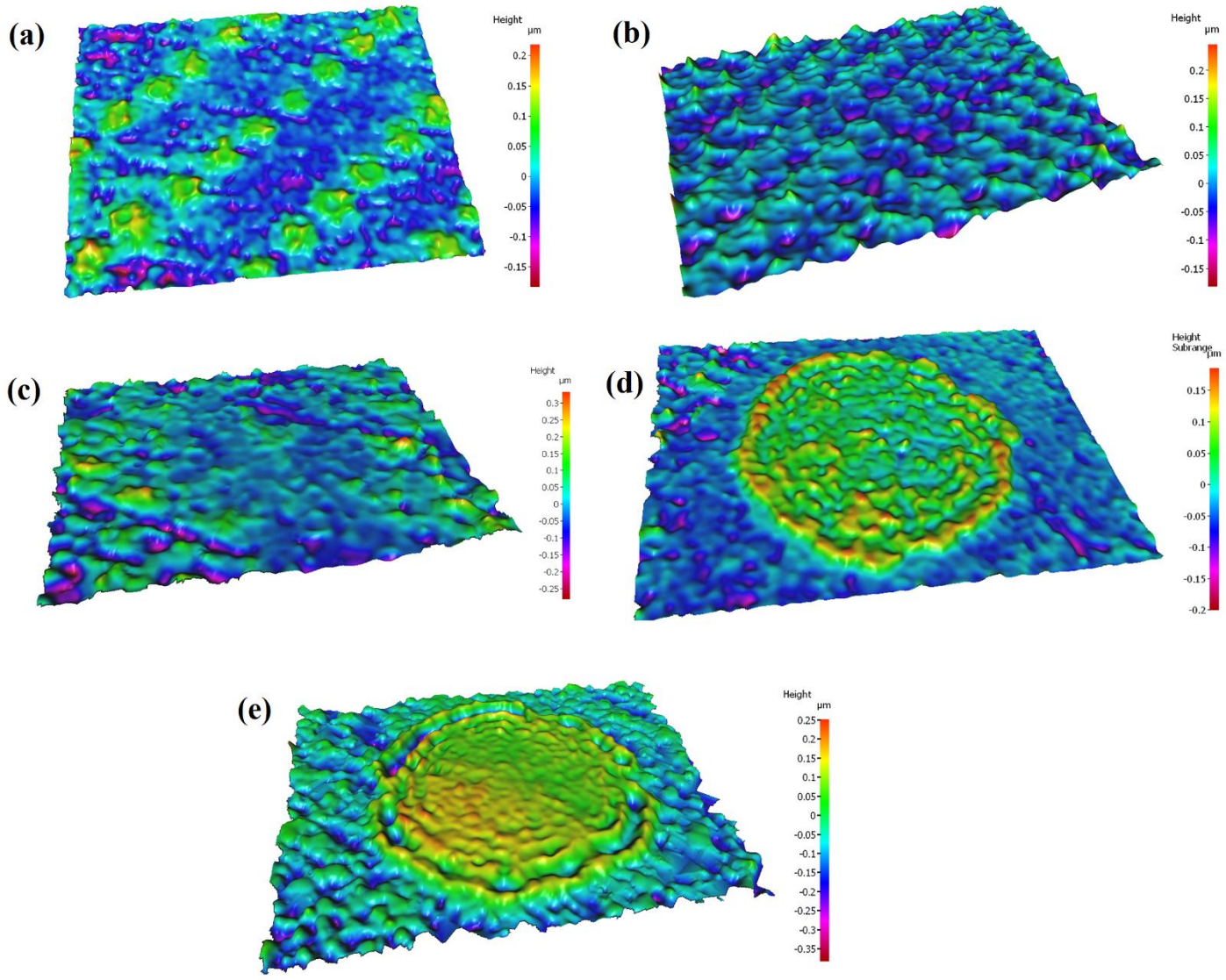

Fig. 6. 3D topographical maps of the treated zones: a) UV1, b) UV2, c) YAG1, d) YAG2 and e) YAG 3, the scanned area is 145 x 110 µm.

Fig. 7 illustrates the comparison of hardness (H) among all the samples, untreated and treated by UV and YAG. In light of the results achieved with Raman analysis, the following changes in the hardness can be discussed:

(i) All "free area" zones show approximately the same H values as the reference, confirming that laser influence was mainly restricted to the incidence zone. The exception of UV2 sample should be attributed to the very small areas of the untreated zones, making difficult to

set the indentation test on them correctly without having influence of the treated zone (see the UV2 micrograph in Fig. 3).

(ii) Generally, the irradiated areas have lower average hardness than those of untreated surfaces, as a result of the structural transformation occurring in the material. This difference was less pronounced for the YAG1 and YAG2 treatments. Considering that the starting amorphous films are biphasic and the laser irradiation promotes the crystallization of WS_2 and also of the graphitisation of carbon phase (typical hardness of graphite is between 0.25 and 0.45 GPa), it is plausible that each one contributes to the overall hardness decrease. However, it is important to emphasize that only under moderate laser irradiation intensity the crystalline WS_2 phase was detected by Raman. The crystallinity of these films can be described as platelets of WS_2, i.e. stacking of a few basal planes (mostly 2-3 planes) with a typical length of ~ 5 nm immersed in an amorphous C-based matrix. According to the literature, such films with nanocomposite structure have hardness values of this order [28]. On the other hand, it should be remarked that changes in the local order of carbon phase is detected by Raman in all treated zones, even on the less irradiated ones. However, the higher radiation intensities produced a reduced intensity of the WS_2 Raman feature along with an obvious graphitisation of the amorphous carbon phase, known to produce a hardness decrease. In fact, in irradiated samples where the carbon structure was not notably affected, the hardness did not change much, regardless the formation of crystalline WS_2. Thus, it seems that the hardness changes are mainly dominated by the carbon matrix contribution.

(iii) The differences in the hardness between treated and untreated zones should be related with the graphitisation degree. UV1 sample has a slightly lower hardness than YAG1 and YAG2, although they show similar Raman spectra, since in the centre (where nanoindentation was performed) of some of the dots, overexposure occurred with stronger graphitisation (see spectrum of point 3-UV1 in Fig. 3).

(iv)The lowest hardness values were measured in UV2 and YAG3 treated zones in good agreement with the strong graphitisation detected by Raman in these zones.

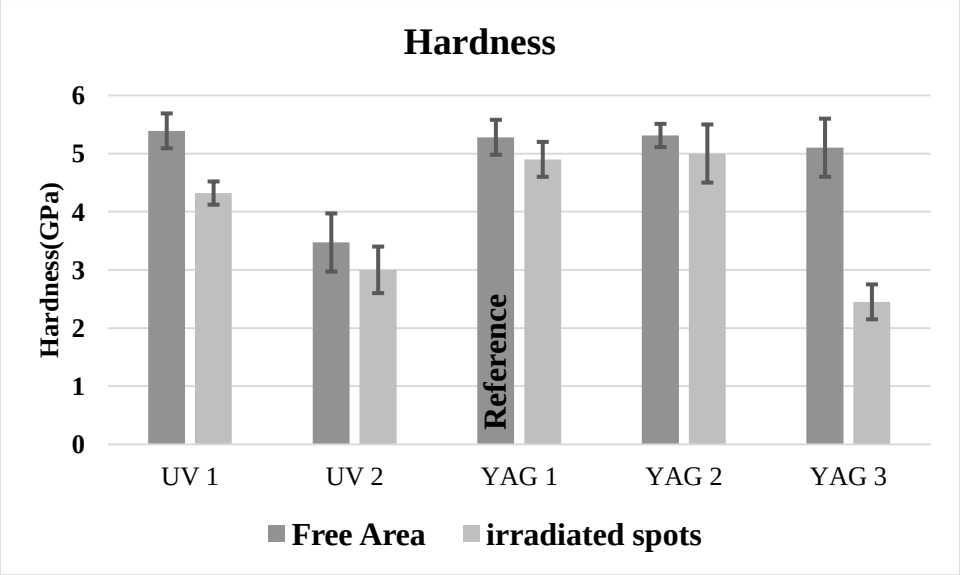

Fig. 7. The comparison of hardness values between untreated and irradiated areas of samples.

3.2. Tribological properties

From a tribological point of view, the formation of a self-adapted tribolayer consisting of well-aligned planes of WS_2, parallel to the sliding direction, has been introduced as the mechanism for self-lubrication in WS_2-based coating [29, 30].

Fig. 8(a) and Fig. 8(b) show the evolution of the coefficient of friction (COF) versus sliding time for all the samples. Generally, two main stages for sliding testing of thin films can be observed in the friction curves, running-in and steady-state. The friction coefficient of the reference sample starts with a high friction coefficient of 0.15. In the running-in stage it continuously drops towards a steady-state value of ~0.08. This can be interpreted by the formation of the above mentioned self-adapted tribolayer. In the case of UV1, YAG1 and YAG2 samples, the running-in stage is very short and the friction coefficient levels out approximately until the end of the test close to ~0.08. The induced crystallization facilitates the reorientation of the WS_2 platelets in the sliding contact allowing to achieve the low friction regime much faster. As can be observed in Fig. 8(a), in the case of UV1, the effects of the laser treatment are, in the end of the test, almost null.

Fig. 9 and Fig. 10 illustrate the micrographs of wear track of UV-laser and YAG-laser treated samples along with their Raman spectra, respectively. With the exception of a small number of dots in UV1 sample, where crystalline WS_2 is still detected (see e.g. point 2-UV1 in Fig. 9), Raman spectra indicate that structure is similar to the untreated zones, either inside or

outside the wear track (see e.g. spectra point 1-UV1 and point 3-UV1, respectively). The wear rates and the average COF are shown in Fig.11. Averaging was performed for the whole duration of the test and the uncertainties presented are from the repetition of the test. The lowest values are observed for the YAG1 and YAG2 treatments, although the latter treatment shows slightly better wear resistance, which can be explained by the best compromise between the hardness values and the structure after laser transformation in these samples. The best compromise is related to the small treated volume of the coating with a treatment inducing crystallization of the WS_2 without significant graphitisation of the a-C phase. This process leads to the generation of small reservoirs of crystalline WS_2 (low shear strength phase) without significantly affecting the untreated areas (load support phase). The depth of the wear tracks (see Table 3) is in all cases close to 0.36 µm, value, which combined to the micrographs of Fig. 1, allows to conclude that the depth of laser treatment should be lower than 0.50 µm for both lasers.

In opposition to the above-described samples, for which the tribological behaviour is mainly determined by the WS_2 phase, in UV2 sample the graphitized material seems to govern the friction phenomena: the response to sliding consists in a rather stable coefficient of friction but following slightly higher values. In the YAG3 sample, the presence of dots with graphitized material also provides a similar behaviour to UV2. Both these samples show a much higher wear rate than the previous ones (see Fig. 10 and Table 3), particularly for UV2, since in this coating the majority of the surface was laser treated. The higher coefficient of friction for the UV2 sample can be related to the lower hardness of the coating caused by the overexposure. It should be noted that the most advantageous sliding scenario would be having low shear strength interface (e.g. WS_2 rich tribofilm) between the surfaces in contact with a harder phase beneath the tribofilms in order to reduce the real area of contact and reduce the ploughing effects [31]. In the case of UV2 sample, the increase in the friction, compared to the YAG3 sample, is related to the increased wear of the coating (see Fig. 11), caused by the excessive transformation and softening of a bigger volume in the coating. For UV2 sample, the structure in the original brighter zones of the wear track, evaluated by Raman, is similar to the reference sample, whereas for the darker one still signs of graphitisation, although not so intense, are detected (see Fig. 9). These results suggest that the increase of the UV laser power pulse from 4 to 30mW, more than double the depth of the treatment, being in the last case higher than 0.9 µm. In the case of YAG3, the laser power influence on the treated depth is also observed, since from YAG2 to YAG3 samples the

decrease in the laser focus distance implies that a higher radiation dose is supplied to the sample. Fig. 10(b) shows that in the wear track there are still well visible laser-induced dots even if the wear track depth is close to 0.5 µm. Raman analysis of these dots shows a variety of structures including graphitisation and WS_2 crystallization, showing different levels of structural transformations depending on the depth at which the analysis is being performed. During each laser pulse, the power delivered to the material reduces as a function of the depth. Then, it is expected that, from the top down to the bulk of the coating, the structural transformation evolves as follows: (i) strong graphitisation occurring close to the surface, (ii) a mixing of graphitisation with WS_2 crystallization and, finally, (iii) WS_2 crystallization and an increase of the order in C-based phase. To get a better understanding of the treatment condition, the schema of a treated sample from cross-sectional view is presented in Fig. 12. In this schema, the value of 'h' is the depth of a treated spot in a sample, which can be imagined as a container with the treated materials. Based on this figure, the volume of the treated zone in a single spot could be divided into two parts, namely A and B, each one corresponding to different levels of laser treatment. It is assumed that these two parts are filled with either similar phases or different ones. For example, in the case of UV 2 and YAG 3, for which different Raman spectra exist before and after sliding, part A would be full of only graphitized material; while part B would be filled by a mixture of graphitic carbon and crystalline WS_2. The top-most graphitised layers are progressively worn during the running-in period until the harder less treated areas are reached. During this time, the lubricious tribofilms are established on both counter bodies, generally resulting in lower running-in times.

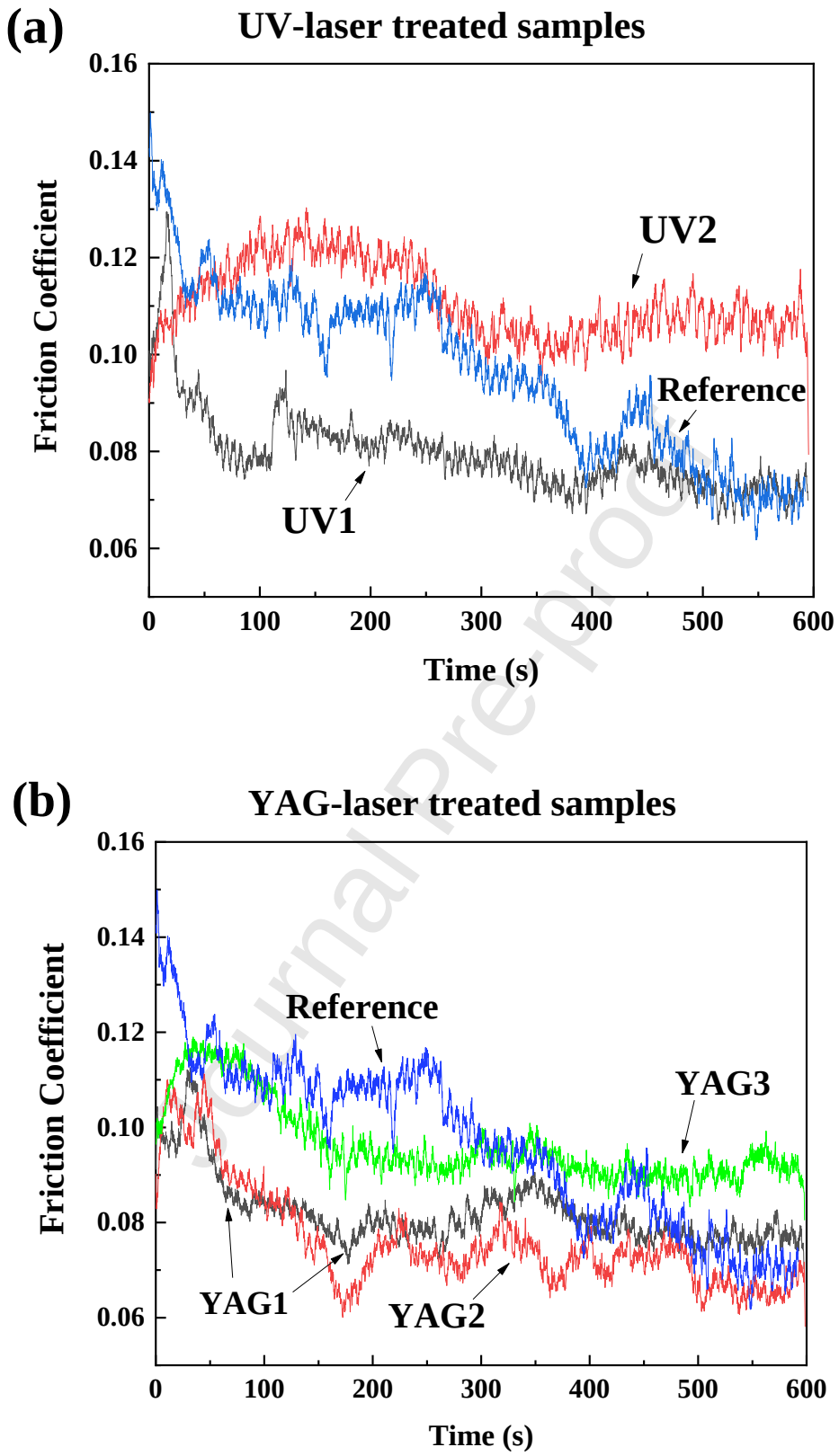

Fig. 8. The friction coefficient versus sliding time of the UV (a) and YAG (b) laser-treated samples in comparison with the reference.

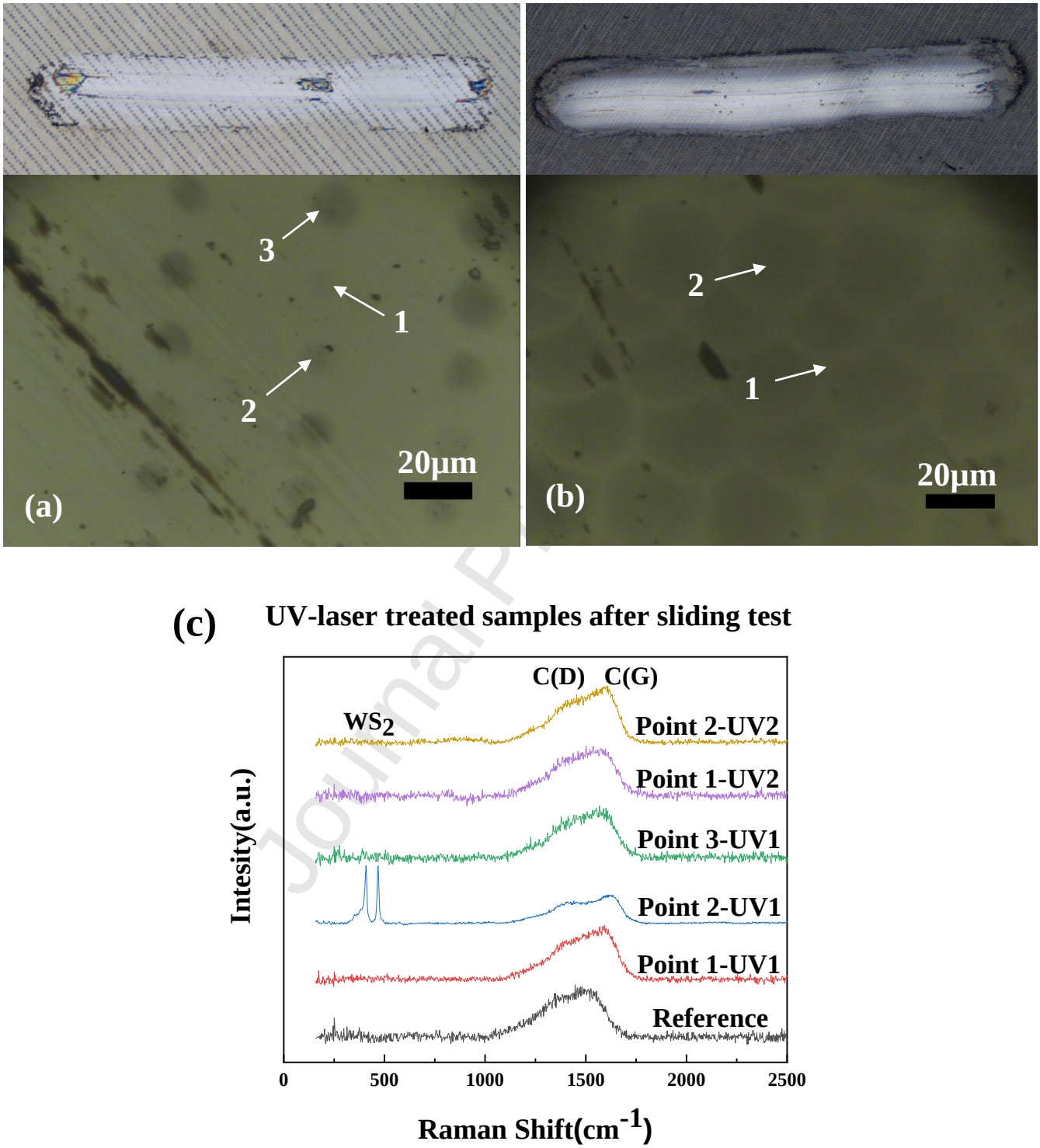

Fig. 9. Micrographs of the wear tracks of UV1 (a) and UV2 (b) along with their Raman spectra (c).

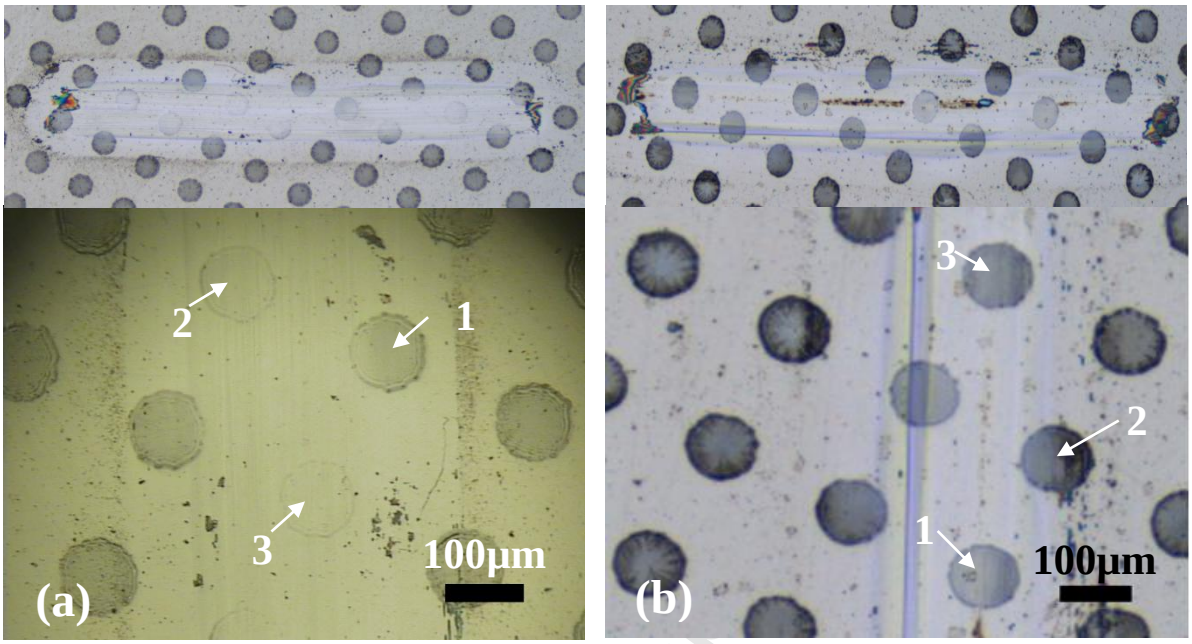

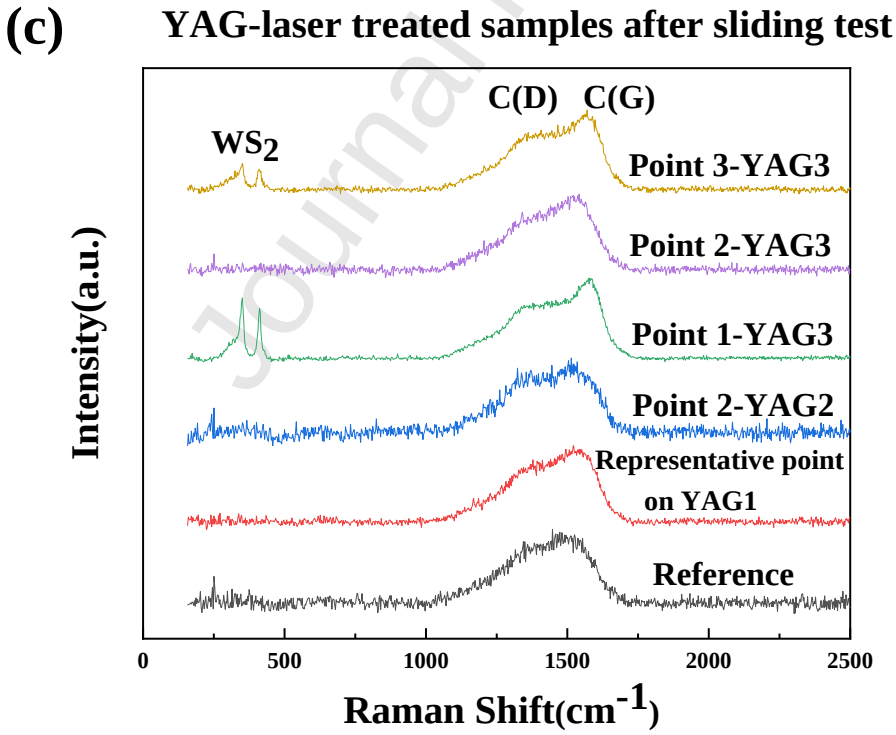

Fig. 10. Micrographs of the wear tracks of YAG2 (a) and YAG3 (b) along with the Raman spectra of all YAG-laser treated samples(c).

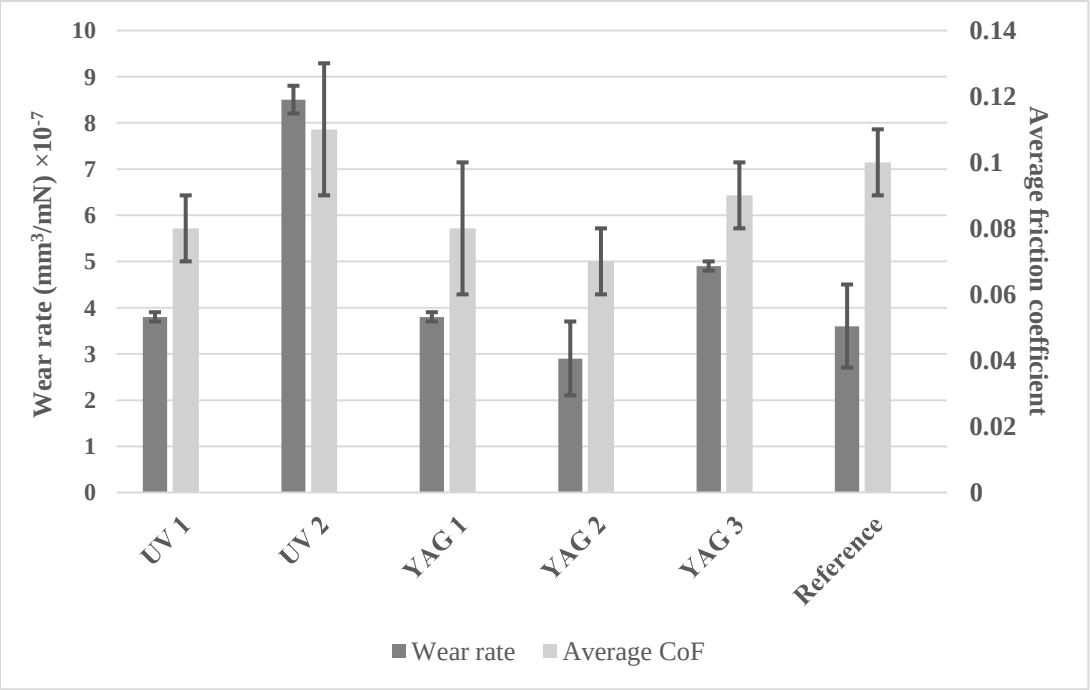

Fig. 11. The average friction coefficient and wear rates of laser-treated samples.

Table 3. The approximate depth of the scars on the samples based on the 3D profilometry performed.

Sample	Reference	UV1	UV2	YAG1	YAG2	YAG3
Depth [µm]	0.36	0.38	0.91	0.36	0.35	0.49

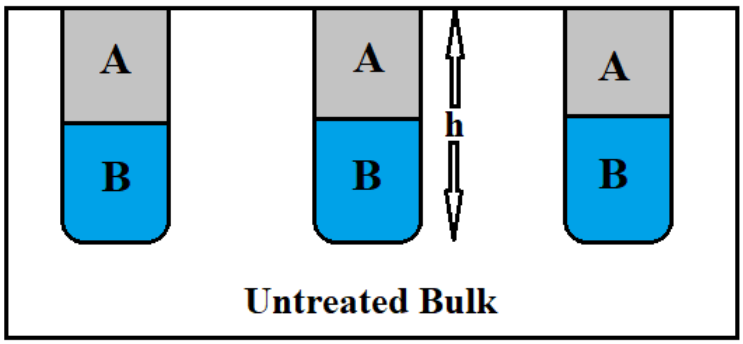

Fig. 12. Schematic cross-section of a treated sample.

4. Conclusion

In this work, W-S coatings alloyed with approximately 50 at. % carbon were deposited by the magnetron sputtering technique, and subjected to five different treatment procedures using pulsed UV and IR (Nd:YAG) lasers.

X-ray diffractometry showed a broad band in the samples' diffractograms, indicating that most of the treated coatings still have an amorphous structure very similar to the reference.

Using Raman spectroscopy, WS_2 crystallization has been confirmed in the samples that were treated under low laser irradiation intensities. However, either the increase of the laser power or the sample approach to the focal plane led to laser over irradiation, resulting in graphitisation and consequently undesirable mechanical and tribological properties.

According to the reciprocating ball-on-disk test, the treatment mainly affected the running-in and early steady-state tribological behaviour, as corroborated by Raman spectroscopy on the scars. In fact, the later stages of tribological tests were quite similar to the reference, meaning that the treatment depth was shallower than the wear scar depth.

Applying high laser power/intensity mostly transformed the amorphous carbon material. This transformation mostly happens in the outer layers, resulting in graphitisation. Since there is a steep decrease in the radiation intensity with depth, the underlying carbon matrix coating remains as in the reference.

Acknowledgements

This research work is supported by the projects: ATRITO-0 [co-financed via FEDER (PT2020) POCI-01-0145-FEDER-030446 and FCT (PIDDAC)], On-SURF [co-financed via FEDER (PT2020) POCI-01-0247-FEDER-024521] and CEMMPRE – UID/EMS/00285/2020 [co-financed via FEDER and FCT (COMPETE)].

The authors also acknowledge all supports from the European Union through the TRIBOS-Erasmus Mundus Joint Master Programme in Tribology of Surfaces and Interfaces as well as the Horizon 2020 research and innovation program under grant agreement No 721642: SOLUTION.

References

Credit Author Statement

Mohammadreza Shamshiri: Writing - Original Draft, Visualization, Formal analysis, Investigation **Ana Manaia:** Conceptualization, Resources **Todor Vuchkov:** Investigation**,** Writing - Review & Editing **Alexandre Carvalho:** Investigation **Guilherme Gaspar:** Investigation **António Fernandes:** Investigation **Samaneh Heydarian Dolatabadi:** Writing - Review & Editing **Florinda Costa:** Methodology, Writing - Review & Editing, Supervision, Funding acquisition **Albano Cavaleiro** Conceptualization, Methodology, Writing - Review & Editing, Supervision, Funding acquisition

Declaration of interests

☒ The authors declare that they have no known competing financial interests or personal relationships that could have appeared to influence the work reported in this paper.

☐The authors declare the following financial interests/personal relationships which may be considered as potential competing interests:

Graphical abstract

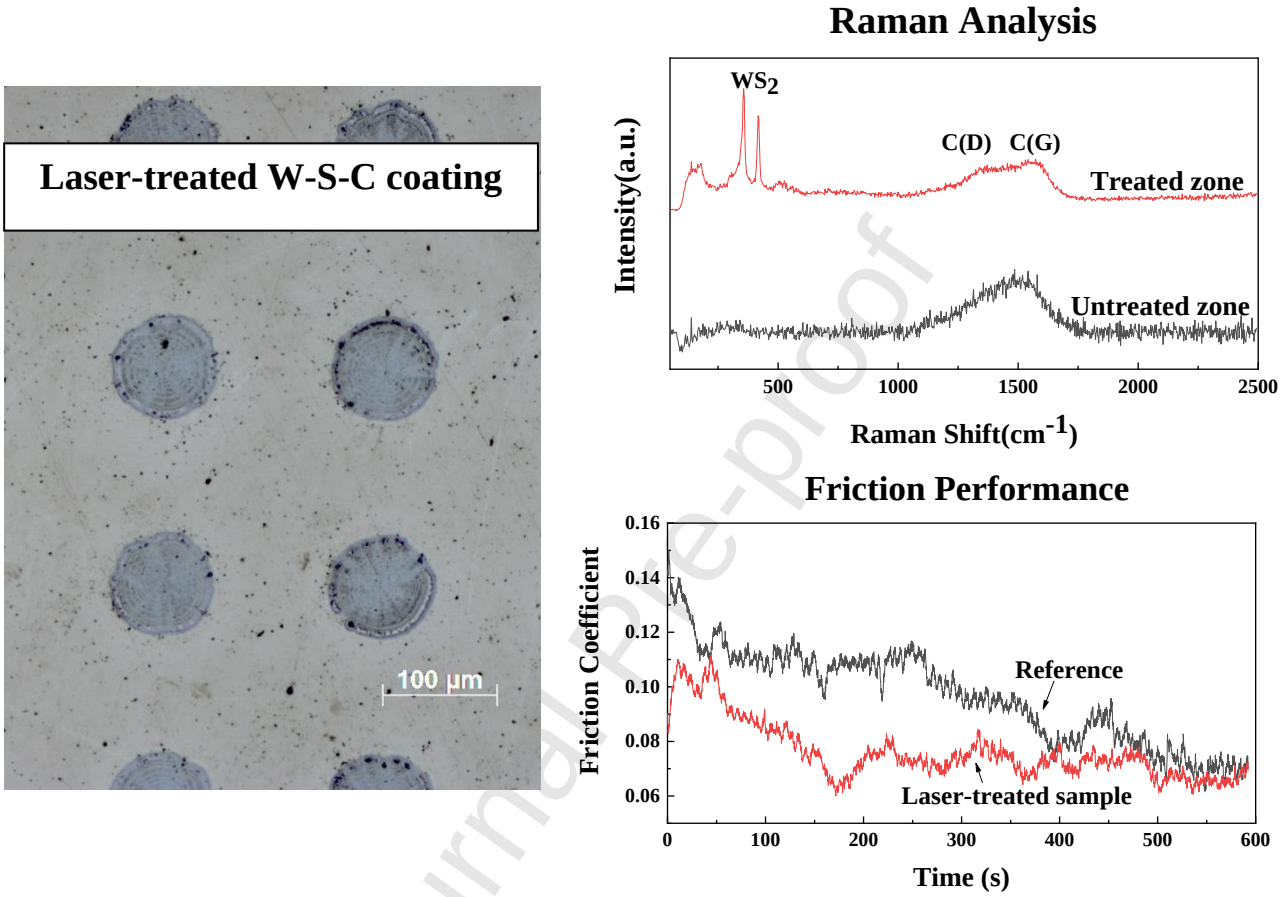

Highlights

- Treatment of W-S-C coatings is possible with low intensity UV and IR lasers.

- Crystallization of originally amorphous W-S coating under moderate laser irradiation intensity.

- Laser irradiation decreases the hardness in treated zones.

- Laser treatment is a way to enhance the tribological performance of W-S-C coating in running-in period.

[1] B. Bhushan, Principles and applications of tribology, second ed., John Wiley & Sons Ltd., New York, 2013.
[2] J. A. Tichy, D. M. Meyer, Review of solid mechanics in tribology, Int. J. Solids Struct. 37 (2000) 391-400. https://doi.org/10.1016/S0020-7683(99)00101-8.
[3] I. L. Singer, Friction and energy dissipation at the atomic scale: A review, J. Vacuum Sci. Techno. A 12 (1994) 2605-2616. https://doi.org/10.1116/1.579079.
[4] P. L. Menezes, P. K. Rohatgi, E. Omrani, Self-Lubricating Composites, first ed., Springer-Verlag Berlin Heidelberg, Berlin, 2018.
[5] T. Polcar, A. Cavaleiro, Review on self-lubricant transition metal dichalcogenide nanocomposite coatings alloyed with carbon, Surf. Coat. Technol. 206 (2011) 686–695. https://doi.org/10.1016/j.surfcoat.2011.03.004.
[6] X. Duan, C. Wang, A. Pan, R. Yu, X. Duan, Two-dimensional transition metal dichalcogenides as atomically thin semiconductors: opportunities and challenges, Chem. Soc. Rev. 44 (2015) 8859-8876. http://dx.doi.org/10.1039/C5CS00507H.
[7] G. H. Han, D. L. Duong, D. H. Keum, S. J. Yun, Y. H. Lee, Van der Waals Metallic Transition Metal Dichalcogenides, Chem. Rev. 118 (2018) 6297-6336. https://doi.org/10.1021/acs.chemrev.7b00618.
[8] T. Polcar, M. Evaristo, A. Cavaleiro, Friction of self-lubricating W-S-C sputtered coatings sliding under increasing load, Plasma Process. Polym. (2007) 541–546. https://doi.org/10.1002/ppap.200731402.
[9] T. W. Scharf, A. Rajendran, R. Banerjee, F. Sequeda, Growth, structure and friction behavior of titanium doped tungsten disulphide (Ti-WS_2) nanocomposite thin films, Thin Solid Films 517 (2009) 5666-5675. https://doi.org/10.1016/j.tsf.2009.02.103.
[10] E. Omrani, P. K. Rohatgi, P. L. Menezes, Tribology and Applications of Self-Lubricating Materials, first ed., CRC Press, Boca Raton, 2017.
[11] T. Polcar, M. Evaristo, A. Cavaleiro, The tribological behavior of W-S-C films in pin-on-disk testing at elevated temperature, Vacuum 81 (2007) 1439-1442. https://doi.org/10.1016/j.vacuum.2007.04.010.
[12] A. Nossa, A. Cavaleiro, Mechanical behaviour of W-S-N and W-S-C sputtered coatings deposited with a Ti interlayer, Surf. Coat. Tech. 163 (2003) 552–560. https://doi.org/10.1016/S0257-8972(02)00622-9.
[13] A. Nossa, A. Cavaleiro, Chemical and physical characterization of C(N)-doped W–S sputtered films, J. Mater. Res., 19 (2004) 2356–2365, https://doi.org/10.1557/JMR.2004.0293.

[14] W. M, Steen, K. Watkins, Coating by laser surface treatment, J. Phys. IV 03 (1993) 581-590. https://doi.org/10.1051/jp4:1993961.
[15] W. M. Steen, J. Mazumder, Laser Processing Material Processing, fourth ed., Springer, London, 2010.
[16] D. Van de Wall, Laser Ablation for Advanced Surface Treatments. Laser Technik J. 14 (2017) 34–37. https://doi.org/10.1002/latj.201700019.
[17] Q. Ding, L. Wang, L. Hu, Tribology optimization by laser surface texturing: from bulk materials to surface coatings, in: J.L.G. Waugh (Ed.), Laser Surface Engineering, Woodhead Publishing, Sawston, 2015, pp. 405–422.
[18] A. Jagminas, G. Niaura, R. Žalnėravičius, R. Trusovas, G. Račiukaitis, V. Jasulaitiene, Laser Light Induced Transformation of Molybdenum Disulphide-Based Nanoplatelet Arrays, Sci. Rep. 6 (2016) 37514. https://doi.org/10.1038/srep37514.
[19] S. J. An, Y. H. Kim, C. Lee, D. Y. Park, M. S. Jeong, Exfoliation of Transition Metal Dichalcogenides by a High-Power Femtosecond Laser, Sci. Rep. 8 (2018) 12957. https://doi.org/10.1038/s41598-018-31374-w.
[20] K. Holmberg, A. Matthews, Coatings Tribology: Properties, Mechanisms, Techniques and Applications in Surface Engineering, second ed., Elsevier, Oxford, 2009.
[21] G. Weise, N. Mattern, H. Hermann, A. Teresiak, I. Bacher, W. Bruckner, H. D. Bauer, H. Vinzelberg, G. Reiss, U. Kreissig, M. Mader, P. Markschlager. Preparation, structure and properties of MoSx films. Thin Solid Films, 298 (1997) 98-106. https://doi.org/10.1016/S0040-6090(96)09165-1.
[22] M. Evaristo, A. Nossa, A. Cavaleiro, W–S–C sputtered films: Influence of the carbon alloying method on the mechanical properties, Surf. Coat. Tech. 200 1-4 (2005) 1076-1079. https://doi.org/10.1016/j.surfcoat.2005.02.039.
[23] T. Vuchkov, M. Evaristo, T. B. Yaqub, A. Cavaleiro, The effect of substrate location on the composition, microstructure and mechano-tribological properties of WSC coatings deposited by magnetron sputtering, Surf. Coat. Tech. 386 (2020) 125481. https://doi.org/10.1016/j.surfcoat.2020.125481.
[24] A. C. Ferrari, J. Robertson, Raman spectroscopy of amorphous, nanostructured, diamond–like carbon, and nanodiamond, Phil. Trans. R. Soc. Lond. A 362 (2004) 2477–2512. https://doi.org/10.1098/rsta.2004.1452.
[25] A.C. Ferrari, J. Robertson, Interpretation of Raman spectra of disordered and amorphous carbon, Phys. Rev. B. 61 (2000) 14095–14107. https://doi.org/10.1103/PhysRevB.61.14095.
[26] A. Berkdemir, H. R. Gutiérrez, A. R. Botello-Méndez, N. Perea-López, A. L. Elías, C. Chia, B. Wang, V. H. Crespi, F. López-Urías, J. Charlier, H. Terrones, M. Terrones Identification of individual and few layers of WS2 using Raman Spectroscopy. Sci. Rep. 3 (2013) 1755. https://doi.org/10.1038/srep01755.
[27] T. V. Kononenko, S. M. Pimenov, V. V. Kononenko, E. V. Zavedeev, V. I. Konov, G. Dumitru, V. Romano, Laser-induced spallation in diamond-like carbon films, Appl. Phys. A 79 (2004) 543–549. https://doi.org/10.1007/s00339-003-2356-5.
[28] M. Evaristo, A. Nossa, A. Cavaleiro, W–S–C sputtered films: Influence of the carbon alloying method on the mechanical properties, Surf. Coatings Technol. 200 (2005) 1076–1079. https://doi.org/10.1016/j.surfcoat.2005.02.039.
[29] A. Erdemir, Solid lubricants and self-lubricating films, in: B. Bhushan, Modern Tribology Handbook, first ed., CRC Press, Boca Raton, 2001, pp.806-808.

[30] G. Stachowiak, A. Batchelor, Engineering Tribology, fourth ed., Butterworth-Heinemann, Oxford, 2014.
[31] D. Tabor, Friction—the present state of our understanding, J. Lubrication Tech. 103(2) (1981) 169-179. https://doi.org/10.1115/1.3251622.